Applied Catalysis B: Environmental 136–137 (2013) 302–307

Contents lists available at SciVerse ScienceDirect

Applied Catalysis B: Environmental

journal homepage: www.elsevier.com/locate/apcatb

Rationales for the selection of the best precursor for potassium doping of cobalt spinel based deN_2O catalyst

G. Maniak [a], P. Stelmachowski [a], A. Kotarba [a,*], Z. Sojka [a], V. Rico-Pérez [b], A. Bueno-López [b]

[a] Faculty of Chemistry, Jagiellonian University, Ingardena 3, 30-060 Krakow, Poland
[b] Department of Inorganic Chemistry, University of Alicante, Ap.99, E-03080 Alicante, Spain

ARTICLE INFO

Article history:
Received 5 November 2012
Received in revised form 22 January 2013
Accepted 28 January 2013
Available online 14 February 2013

Keywords:
Cobalt spinel
Co_3O_4
N_2O decomposition
Potassium promotion
Potassium precursor
Nitrous oxide
Catalyst
Promoter dispersion
Isotopic labeling
Isotopic pulse
Work function

ABSTRACT

Cobalt spinel Co_3O_4 catalysts promoted with different potassium precursors (K_2CO_3, KNO_3, CH_3COOK, KOH) were prepared and characterized by surface (XPS, work function, SEM) and structure (Raman, XRD, H_2-TPR) sensitive techniques. The stability of potassium promoter was determined by means of Species Resolved-Thermal Alkali Desorption method (SR-TAD). The N_2O decomposition mechanism on series of synthesized catalysts was studied by temperature programmed reaction and pulse experiments of isotopically labeled $^{15}N_2{}^{18}O$. The role of the octahedral cobalt ions as catalytic active sites was revealed. The most dispersed state of alkali promoter, obtained from K_2CO_3 precursor, results in its highest stability and lowest work function, leading to the highest catalytic activity in N_2O decomposition in the investigated K-Co_3O_4 series. The beneficial effect of potassium is discussed in terms of the facile activation of N_2O via dissociative electron transfer ($N_2O + e^- = N_2 + O^-$) and promotion of the preferred fast suprafacial recombination of oxygen intermediates (revealed by the isotopic experiments).

1. Introduction

Catalytic removal of nitrous oxide from anthropogenic sources is a subject of continuous intensive investigations due to its significant global warming potential (310 times larger than that of CO_2), and its contribution to destruction of the ozone layer in the stratosphere [1]. The most significant production of N_2O comes from adipic and nitric acid plants. In the case of the former, due to high concentration of nitrous oxide in the tail gases and the exothermal effect of its decomposition, effective abatement systems have been already developed [2]. On the contrary, the low concentration of the pollutant and the presence of inhibiting co-reactants in the feed gas, such as H_2O, O_2 and NO_x in the feed gases in the nitric acid plant make catalytic removal of N_2O still an unsolved problem [3].

So far, one of the most promising systems for the low temperature catalytic N_2O removal is a modified cobalt spinel. Improvement of its catalytic performance may be achieved by a bulk modification (doping with alien cations) [4–6] or by tuning the surface properties of the catalyst with alkali promoters [7,8]. The latter effect is stronger and results in a dramatic lowering of the reaction temperature even by 200 °C. In our previous papers we have shown that this effect is mainly of electronic origin and is associated with the surface species without invoking previously suggested diffusion of alkali ions into the catalyst bulk [9,10]. Alkali promoters present on the catalyst surface lower the work function of the cobalt spinel facilitating redox processes that occur between the catalyst surface and the reaction oxygen intermediates produced during the N_2O decomposition. The comparison of the effect of different alkali promoters on Co_3O_4 activity in N_2O decomposition presented in our previous work [9] indicates that the beneficial influence of dopants on the catalyst activity increases in the order: Li « Na < K < Cs. It has been reported that the promotional effect of alkali is also present on other oxide catalysts, such as binary 3d transition metal oxides [11], ternary oxides of spinel structure [12] and more complex systems like mixed oxides prepared by thermal treatment of hydrotalcites [13,14]. Thus, the promotional effect appears to be of a more general nature. Recently, the effect of potassium precursors on the catalytic activity of K-promoted NiAl mixed oxides was investigated [14] and it was shown that it depends on the type of potassium precursor. However, the understanding of this strong phenomenon is still lacking.

* Corresponding author at: Faculty of Chemistry, Jagiellonian University, ul. Ingardena 3, 30-060 Krakow, Poland, Tel.: +48 12 6632246; fax: +48 12 6340515.
E-mail address: kotarba@chemia.uj.edu.pl (A. Kotarba).

0926-3373/$ – see front matter © 2013 Elsevier B.V. All rights reserved.
http://dx.doi.org/10.1016/j.apcatb.2013.01.068

In this paper, the effect of potassium precursor nature on the catalytic activity of K-promoted cobalt spinel for N_2O decomposition was systematically examined. The influence of promotion on the two most demanding steps of N_2O decomposition over Co_3O_4: N_2O activation via electron transfer and surface oxygen recombination, is addressed. The aim of this study was to provide rationale basis for selection of the best precursor for potassium doping of cobalt spinel based catalysts in order to reach the highest deN_2O performance.

2. Experimental

2.1. Catalysts preparation

The samples were prepared by incipient wetness impregnation of commercially available Co_3O_4 (Fluka, 16 m^2/g) with different potassium compounds: K_2CO_3, KNO_3, KOH and CH_3COOK. The impregnation procedure was identical for all the investigated samples: 1.60 g of the cobalt spinel was impregnated with 1.2 ml of potassium solution to achieve the surface coverage of 2 atoms/nm^2 (0.2 wt.%). We found such level of potassium doping to be optimal for the K-Co_3O_4 catalyst. The samples were next dried at 100 °C for 1 h and finally calcined at 400 °C for 4 h. As inferred from the BET measurements the impregnation of cobalt spinel with different potassium precursors did not influence its specific surface area in an appreciable way.

2.2. Catalysts characterization

XRD patterns were recorded on a Philips X'Pert APD powder diffractometer with Cu Kα radiation at 10 mA and 10 kV, 2θ step scans of 0.02° and a counting time of 1 s per step. The analysis of catalysts morphology and composition was investigated with the use of Quanta 3D-FEG electron microscope equipped with a EDX analyzer (FEI).

Temperature programmed reduction by H_2 of the catalysts was carried out in a Micromeritics Pulse ChemiSorb 2705 device with a thermal conductivity detector (TCD). The tests were performed in a tubular quartz reactor in the range of 20–600 °C (10 °C/min) with the use of 20 mg of fresh catalyst, flow rate of the feed (5% H_2 in Ar) 40 ml/min. A cold trap was placed before the TCD, consisting of a mixture of isopropyl alcohol and liquid nitrogen (temperature −89 °C).

The Raman spectra recorded at room temperature in ambient conditions were taken using a Renishaw InVia spectrometer equipped with a Leica DMLM confocal microscope and a CCD detector with an excitation wavelength of 785 nm. The laser power at the sample position was about 2.5 mW for magnification of 5×, whereas for 100× magnification the power was set to 0.25 mW. The Raman scattered light was collected in the spectral range 150–850 cm^{-1}. At least six scans were accumulated to ensure a sufficient signal to noise ratio.

Relative bulk amounts of cobalt and potassium were determined with the use of Energy-Dispersive XRF spectrometer (Thermo Scientific, ARL QUANT'X). Samples were in form of pellets of 10 mm in diameter. X-rays in the range of 4–50 kV (1 kV step) were generated with the use of Rh anode, the beam size was 1 mm and the window was made of beryllium. Detector used was 3.5 mm Si(Li) drifted crystal with Peltier cooling (∼185 K). For quantitative analysis an UniQuant software was used with a series of metallic standards.

Work function measurements were carried out under the vacuum of 10^{-7} mbar with the use of the samples pressed into pellets (diameter 10 mm, 8 MPa). To standardize the surface the samples were heated to 400 °C for 15 min. The contact potential difference (V_{CPD}) measurements were carried out by the dynamic condenser method of Kelvin with a KP6500 probe (McAllister Technical Services) at 150 °C. The reference electrode was a standard stainless steel plate with diameter of 3 mm (Φ_{ref} = 4.1 eV) provided by the manufacturer. The work function values were obtained as $eV_{CPD} = \Phi_{ref} - \Phi_{sample}$.

The X-ray photoelectron spectra (XPS) of as obtained samples were measured with a Prevac photoelectron spectrometer equipped with a hemispherical VG SCIENTA R3000 analyzer. The photoelectron spectra were measured using a monochromatized aluminum Al Kα source (E = 1486.6 eV) and a low energy electron flood gun (FS40A-PS) to compensate the residual charge on the surface. The base pressure in the analysis chamber during the measurements was 5×10^{-9} mbar. Spectra were recorded with constant pass energy of 100 eV for the survey and narrow scan spectra.

The stability of potassium promoters was determined by means of Species Resolved-Thermal Alkali Desorption method described in detail elsewhere [15]. For comprehensive characterization of potassium surface stability, both K and K^+ desorption fluxes were measured as a function of temperature with the use of a surface ionization detector.

2.3. N_2O decomposition tests

Temperature programmed reaction (TPR) studies of N_2O decomposition were performed in a quartz flow reactor in the range of 20–600 °C (10 °C/min) with the use of 300 mg of the catalyst (sieve fraction of 0.2–0.3 mm), flow rate of the feed (5% N_2O in Ar) of 7000 h^{-1}. The reaction progress was monitored with a quadruple mass spectrometer (RGA200, SRS, lines for m/z = 44, 32, 28, 30 and 18, corresponding to N_2O, O_2, NO, N_2 and H_2O). The catalytic tests were always performed in at least two consecutive runs and in all cases the results were reproducible. Furthermore, the stability tests for 10 h confirmed that no appreciable deterioration of the catalyst performance takes place.

The experimental data of TPR measurements, expressed as N_2O conversion (X_{N_2O}) versus temperature (T), were fitted with the kinetic model for the flow reactor with quasi ideal mixing, where $k\tau = X/(1-X)$ [16], in order to determine the kinetic parameters, such as rate constants (k) at 400 °C of N_2O decomposition and apparent activation energies (E_a/kJ mol^{-1}) using the Arrhenius formula $k = A \cdot e^{-\frac{E_a}{RT}}$, R – gas constant [kJ/(mol K)]. Moreover, to ensure that the reactor is operating in the kinetic regime, the criterial numbers for extra- and intragranular diffusion limitations were checked according to the eurokin procedure [17]. The obtained parameters are in agreement with those reported in the literature for similar systems [18]. The first order kinetics was assumed on the basis of analysis of molecular level mechanistic considerations of N_2O decomposition [19], which are supported by available experimental data [3,20].

Pulse isotopic deN_2O experiments were carried out in a 5-mm i.d. cylindrical fixed-bed reactor with 50 mg of fresh catalyst packed between plugs of quartz wool. A carrier helium flow rate of 8 ml/min was continuously fed to the reactor, in which Ar or $^{15}N_2{}^{18}O$ were pulsed. A 100 μl volume loop was used to pulse gases (Ar or $^{15}N_2{}^{18}O$) at a pressure of 5 psi (∼0.34 atm) while the carrier helium flow was by passed directly through the reactor. A six-way valve sends the helium flow throughout the loop and sweeps the inside gas to the reactor. The experimental procedure consisted of three steps: (i) pretreatment of the catalyst in air at 400 °C to clean the surface; (ii) injection of three pulses of Ar into helium feed to ensure reproducible profiles (iii) injection of three pulses of $^{15}N_2{}^{18}O$ (Isotec, min 98% ^{15}N, min 95% ^{18}O) at 400 °C. The shape of the Ar profiles provided a reference of the interaction of a non-reactive molecule with the catalyst bed. The gas composition

Table 1
Kinetic parameters for N_2O decomposition over K-promoted Co_3O_4 with different potassium precursors used and their work function.

	E_a (kJ mol^{-1})	k_{400} (m^3 g^{-1} s^{-1})	r_{400} (μmol$_{N_2O}$ m^{-2} s^{-1})	Work function, Φ (eV)
Undoped Co_3O_4	104.6 ± 2.6	$2.3 \pm 0.13 \times 10^{-6}$	0.137	3.84
KNO_3/Co_3O_4	74.1 ± 6.1	$4.8 \pm 0.19 \times 10^{-6}$	0.148	3.71
CH_3COOK/Co_3O_4	69.8 ± 4.0	$4.4 \pm 0.17 \times 10^{-6}$	0.152	3.81
KOH/Co_3O_4	51.5 ± 7.7	$1.0 \pm 0.03 \times 10^{-5}$	0.191	3.67
K_2CO_3/Co_3O_4	36.4 ± 3.1	$2.4 \pm 0.14 \times 10^{-5}$	0.227	3.67

was monitored with a mass spectrometer Pfeiffer Vacuum (model OmniStar), operating at frequency of 1 Hz.

3. Results and discussion

3.1. N_2O decomposition tests

The kinetic parameters obtained from the analysis of the N_2O conversion data (Supplementary data, Fig. S1) and the reaction rates (expressed as number of N_2O molecules decomposed at the catalyst surface of 1 m^2 during one second) are summarized in Table 1. It can be inferred that the apparent activation barriers are lowered upon K-doping and consequently the corresponding rate constants and reaction rates increased substantially. For the bare Co_3O_4 catalyst E_a = 104.6 kJ mol^{-1} and $k_{400} = 2.3 \times 10^{-6}$ m^3 g^{-1} s^{-1} were the highest and the lowest, respectively, in the investigated series. The lowest apparent activation energy of 36.4 kJ mol^{-1}, corresponding to the highest rate constant of 2.4×10^{-5} m^3 g^{-1} s^{-1}, was obtained for the Co_3O_4 catalyst doped with potassium carbonate. There is also a strong improvement of kinetic parameters upon doping with KOH, whereas the promotional effects for KNO_3 and CH_3COOK are much less pronounced (Table 1).

3.2. Bulk characterization

The structural refinement of the XRD patterns (Supplementary data, Fig. S2) of the promoted cobalt spinel samples was performed with the Maud software [21]. The positions of the oxygen anions in the unit cell is specifically defined by the parameter u, which equals to 0.25 for the ideal spinel structure, while for the actual spinel samples it varies in the range $0.24 < u < 0.275$. With the increase of u, the anions move away from the nearest tetrahedral cation in the [1 1 1] direction, which increases the volume of the void, but does not alter its symmetry. Simultaneously, the reduction of the size and symmetry of octahedral voids take place. The optimized cell parameter, a, and position of the oxygen within the unit cell, u, are presented in Table 2. The minor variations of u indicate that the geometrical deformation of the cobalt octahedral are rather small.

The SEM studies of K-doped cobalt spinel catalysts obtained with different potassium precursors have shown that potassium doping does not influence the morphology of Co_3O_4 catalyst in an appreciable way. This suggests that the distribution of potassium additives is restricted to the surface, as confirmed by further spectroscopic studies. The representative SEM images of the investigated catalysts shown in Fig. 1, indicate that the size of the aggregated crystallites is in the range of 50–150 nm. SEM pictures of the Co_3O_4 catalyst and K-Co_3O_4 catalysts doped with KOH, CH_3COOK, KNO_3, K_2CO_3 are quite similar (Supplementary data, Fig. S3). The ED-XRF studies proved that the amount of introduced potassium was similar for all the samples and the atomic ratio, K/(Co + K), equaled to 0.15–0.17%.

The reducibility of the cobalt spinel promoted with various potassium precursors was analyzed by H_2-TPR (Fig. 2). The low temperature shoulder, at $T < 400$ °C, can be attributed to the reduction of Co^{3+} to Co^{2+} and the main peak at $T > 400$ °C to the reduction of bulk Co^{2+} to Co^0 [22,23]. In the case of cobalt spinel promoted with potassium carbonate, the temperature of the first step of reduction moved notably to a lower value upon doping, as observed before elsewhere [8,14]. Those authors correlate the improved cobalt spinel reducibility with the enhancement of the catalytic performance. The obtained results are in line with this suggestion, since the highest effect was observed by us for K_2CO_3 (Table 1). For the remaining catalysts, prepared with other potassium precursors, again, the reducibility decreases together with the lowering of their deN_2O activity.

3.3. Spectroscopic Raman characterization

The Raman spectra of Co_3O_4 and potassium promoted Co_3O_4 reveal five Raman peaks (Supplementary data, Fig. S4). They are located near 194, 473, 515, 612 and 690 cm^{-1} and correspond to the E_g, $3F_{2g}$ and A_{1g} modes of crystalline Co_3O_4, respectively [24]. Potassium promoted spinels show similar Raman spectra with that of unpromoted Co_3O_4, but the vibrations are distinctly shifted to higher frequencies. Further Raman investigations were performed in the ambient conditions at 100× magnification (laser spot radius 560 nm). In all cases, the small shift in the peak positions with

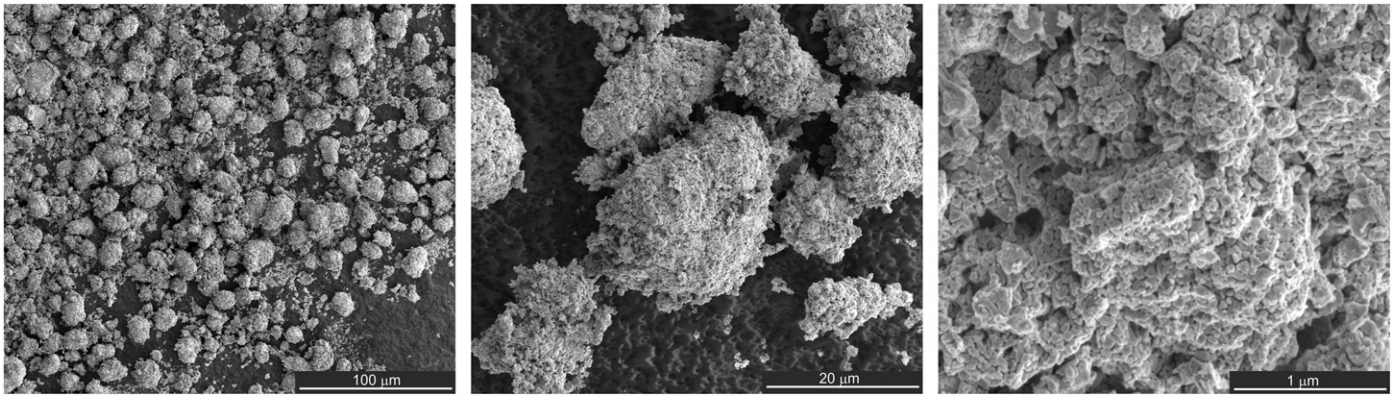

Fig. 1. SEM pictures of the catalyst doped with K_2CO_3 taken at different magnifications.

Table 2
Structural (XRD) and spectroscopic (Raman) parameters of the investigated samples along with the atomic potassium desorption flux (j_K) at 700 °C.

	Cell length, a (Å)	Oxygen position (u)	A_{1g} average band position(cm^{-1})	j_K (nA)
Undoped Co_3O_4	8.085	0.264	689.0	–
KNO_3/Co_3O_4	8.084	0.266	689.4	2.2
CH_3COOK/Co_3O_4	8.084	0.266	689.4	11.4
KOH/Co_3O_4	8.085	0.265	689.9	11.0
K_2CO_3/Co_3O_4	8.086	0.265	690.8	0.05

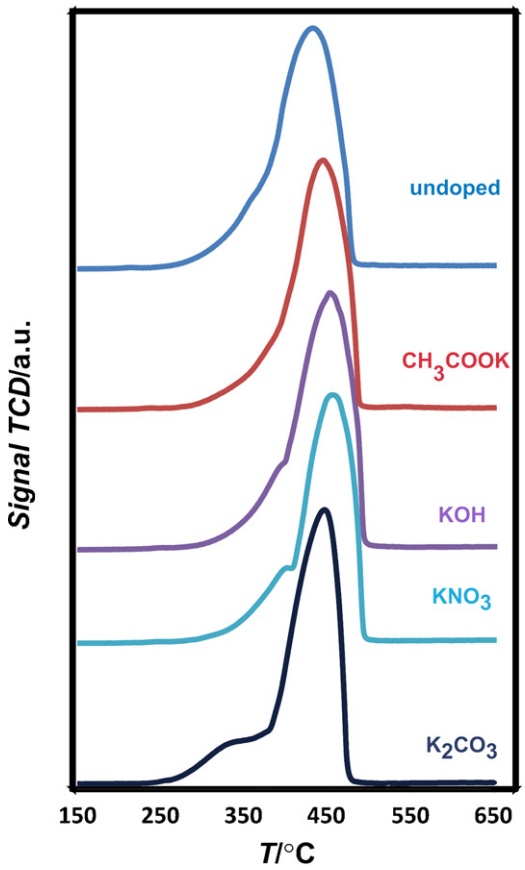

Fig. 2. H_2-TPR profiles for K-doped cobalt spinel catalysts prepared with various potassium precursors.

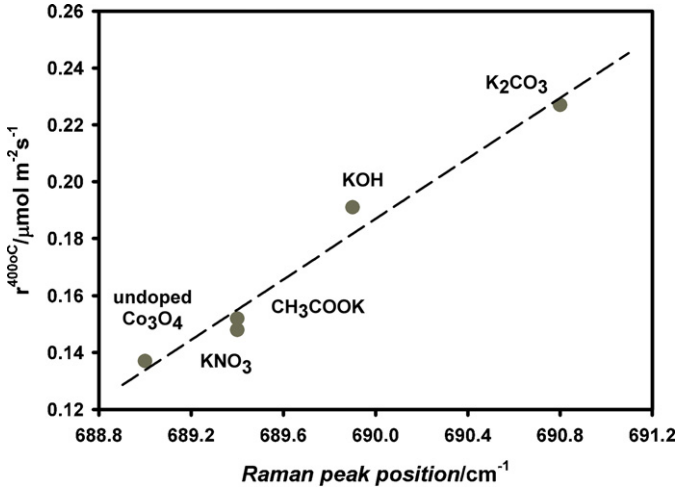

Fig. 3. Reaction rate at 400 °C versus Raman peak positions around 690 cm^{-1}, related to the octahedral cobalt—oxygen bond, for Co_3O_4 promoted with potassium from different precursors.

respect to unpromoted Co_3O_4 becomes evident (A_{1g} at ~692 cm^{-1}). To ensure the representative value of the A_{1g} peak position, the spectra were taken from at least five random spots from the powder material. As in the other normal spinel oxides, the spectral region 600–700 cm^{-1} is characteristic of vibrations involving the motion of oxygen atoms on the corners of the octahedral unit [25,26]. The average wavelength of the A_{1g} mode can be thus used as an indicator of the perturbation of the breathing vibration of the Co_{Oh}—O bond upon K-doping (Table 2). These results are consistent with the reported influence of the surface potassium on the A_{1g} band position of the cobalt spinel [23], and are in line with the improved reducibility of Co_3O_4 by addition of potassium as revealed in H_2-TPR profiles (Fig. 2). Indeed, the low temperature peak is associated with the octahedral Co^{3+} reduction to Co^{2+} and the effect of potassium is the most pronounced for the K_2CO_3 sample, for which the highest Raman shift was observed. The Raman shift of the A_{1g} vibration of the octahedral cobalt is also clearly correlated with the catalyst reactivity (Fig. 3), indicating that the octahedral Co^{3+} cations are definitely the active sites for N_2O decomposition. The perturbation of cobalt octahedral by potassium is evidently reflected in the twofold changes in the reaction rate for the optimal potassium carbonate precursor. Indeed, in our previous work [27] on the basis of spectroscopic results by site selective substitution and catalytic data it has been shown that the Co^{3+} ions in the octahedral positions are mainly responsible for the catalytic activity of Co-spinels in deN2O reaction, whereas, the substitution of Co^{2+} in tetrahedral sites has relatively small influence on the increase of the reactivity in comparison with octahedral substitution.

3.4. Work function and XPS characterization

The analysis of the area of Co2p, O1s, K2p and C1s photopeaks (Supplementary data, Fig. S5) allowed for determination of the surface composition of the as-prepared samples (K/Co in Fig. 5). Although during the synthesis equal amounts of potassium were introduced into the spinel samples, the XPS measurements show large variation of the surface K/Co ratio (despite that the total content of potassium was the same as revealed by XRF measurements). These results can be accounted for by a different dispersion of potassium on the surface of investigated spinel catalysts depending on the precursor nature (vide infra).

Since it was previously found that the catalytic activity correlates with the electronic properties of the catalyst surface [9,10,12,27], the influence of potassium doping on work function was examined. In this study a strong correlation between the kinetic parameters and the work function values was also observed. This is illustrated in Fig. 4, where the reaction rate and temperature of 50% conversion of N_2O decomposition are plotted against the catalyst work function for various potassium precursors. The highest decrease of work function obtained upon doping of cobalt spinel with potassium carbonate corresponds to the highest increase of the catalytic deN_2O activity.

Potassium, due to its low ionization potential, transfers charge to the catalyst and by formation of the $K^{\delta+}$—$O_{surf}^{\delta-}$ surface dipoles modifies the catalyst work function significantly [10]. Different level of the observed promotional effect for various potassium

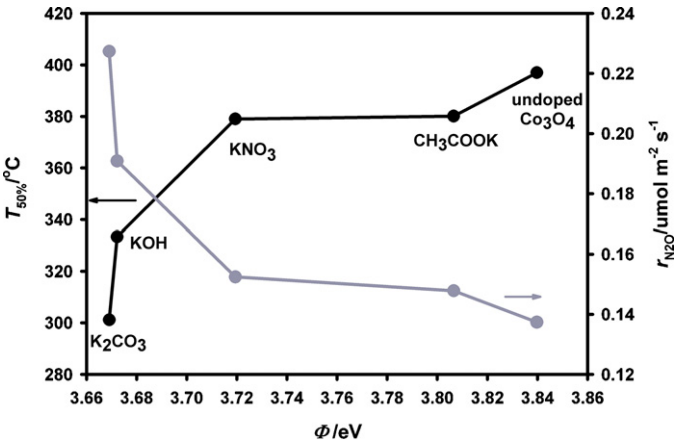

Fig. 4. Catalytic activity represented by reaction rate (top) and half conversion temperature of N_2O decomposition ($T_{50\%}$; bottom) against the catalyst work function (Φ) for K-promoted cobalt spinel obtained with different potassium precursors.

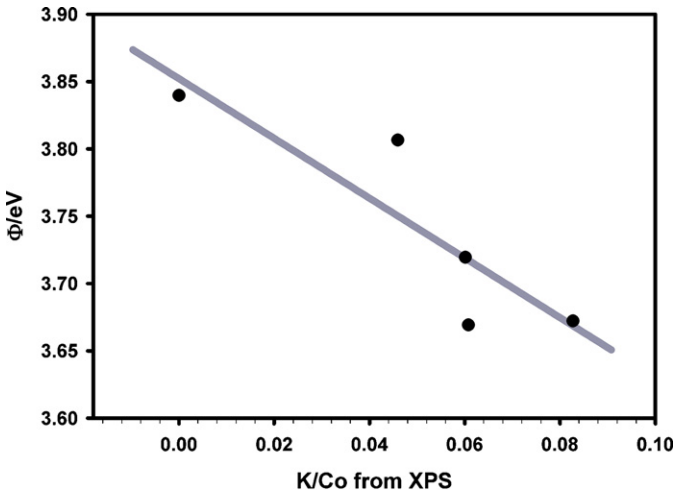

Fig. 5. Work function versus surface potassium/cobalt (K/Co) ratio.

precursors can be explained by different surface stability and/or dispersion of the resultant potassium species formed upon thermal pre-treatment of the samples. The stability of potassium surface species was examined by the thermal desorption experiments. The atomic potassium desorption flux measured at 700 °C showed from tens to hundreds times lower intensity for K_2CO_3/Co_3O_4 sample than for other potassium precursors (Table 2).

The correlation of work function of metal oxides with standard enthalpy of its formation was reported in the literature [28]. According to this study, the lower work function the lower enthalpy and the easier oxygen release. Thus, the correlation of electronic properties, reactivity and reducibility are experimentally supported.

The cationic redox mechanism of deN_2O reaction over cobalt spinel consists in three general steps: N_2O molecule activation by electron transfer ($N_2O + e^- = N_2 + O^-$), diffusion of adsorbed surface oxygen, and recombination of the latter with dioxygen desorption [29]. Since all these steps exhibit a redox character, they strongly depend on the electronic properties of the catalyst surface. The calculated activation energies of the first and the last steps are equal to 84 and 96 kcal/mol over the model (1 0 0) cobalt spinel surface [30]. The explanation, based on the experimental results, takes into account that the electron transfer from the surface to the N_2O molecule, which initiates the N—O bond cleavage, should be facilitated by the work function lowering.

The relation of surface potassium concentration and the catalyst work function is shown in Fig. 5. It can be observed that increase of the XPS detected potassium/cobalt ratio coincides monotonously with the decrease of the catalyst work function. Taking into account the equal doping level, the actual surface potassium content reflects different degree of its agglomeration. Thus, the clear advantage of using K_2CO_3 as a potassium precursor consists in better stability and improved dispersion of the promoter, leading to strongest decrease of the spinel work function, which through correlation shown in Fig. 4 is beneficial for the catalyst activity.

3.5. Isotopic pulse experiments

The pulse experiments performed with isotopically labeled nitrous oxide ($^{15}N_2{}^{18}O$) provided information about the effect of potassium doping on N_2O decomposition mechanism. The reactant profiles obtained in these experiments with bare and K_2CO_3-promoted Co_3O_4 are plotted in Fig. 6. The K_2CO_3-promoted Co_3O_4 catalyst decomposed all $^{15}N_2{}^{18}O$ pulsed at 400 °C, while in the case of the bare Co_3O_4 catalyst only a half of the molecules were converted. This is in agreement with the TPR test results as can be

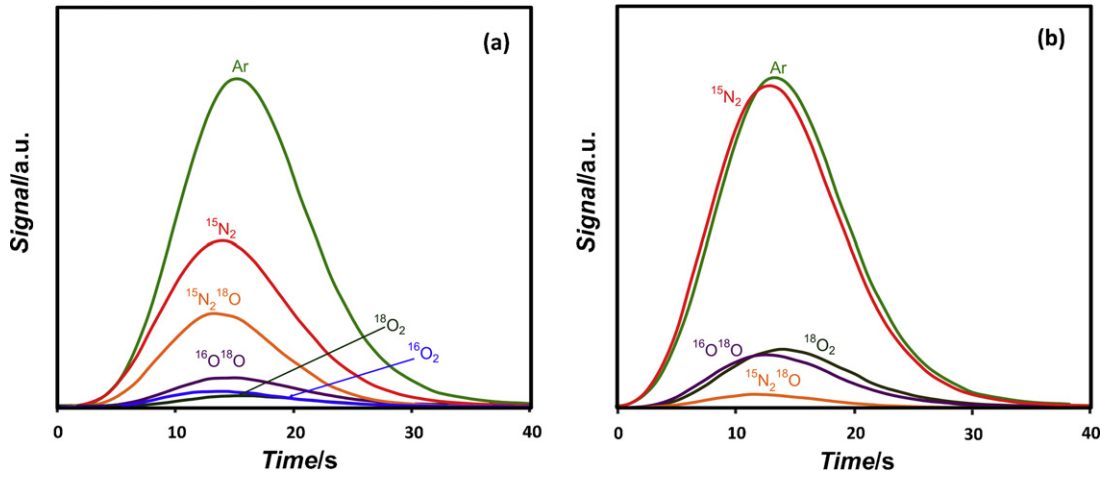

Fig. 6. Gas profiles obtained in pulse experiments performed with Ar and $^{15}N_2{}^{18}O$ at 400 °C over Co_3O_4 (a) and K_2CO_3-promoted Co_3O_4 (b).

inferred from the data in Table 1. As can be observed in Fig. 6b, the $^{15}N_2$ and Ar profiles are quite similar, indicating that N_2 molecules are not accumulated on the catalyst upon N_2O decomposition, but they are released immediately, without any delay with respect to the Ar inert gas profile. Further information is obtained from the O_2 products distribution ($^{18}O_2$, $^{18}O^{16}O$ and $^{16}O_2$). The $^{18}O_2$ product comes from the decomposition of $^{15}N_2{}^{18}O$ on octahedral cobalt sites of the catalyst and further recombination of the superfacial ^{18}O atoms. The $^{18}O^{16}O$ isotopomer is produced from the ^{16}O-surface sites and superfacial ^{18}O (ex $^{15}N_2{}^{18}O$), whereas $^{16}O_2$ originates from the recombination of catalyst surface oxygen atoms only. The position of the maximum level in the $^{18}O^{16}O$ profiles is equal to that of $^{15}N_2$ and $^{15}N_2{}^{18}O$, while that $^{18}O_2$ needs some more time to release. The K_2CO_3-promoted catalyst only yielded $^{18}O_2$ and $^{18}O^{16}O$, while the bare Co_3O_4 catalyst additionally produced $^{16}O_2$.

The ratio of the $^{18}O_2$ and $^{16}O^{18}O$ signals from the pulse experiments indicates that in the case of potassium promoted Co_3O_4 the relative amount of surface ^{16}O oxygen in the reaction products is much lower than in the case of bare Co_3O_4. The recombination of oxygen is found to be one of the key steps during the N_2O decomposition over cobalt spinel [10], thus the facilitation of dioxygen formation and its subsequent desorption by potassium promotion substantially enhanced the reactivity of Co_3O_4. The promotional effect of potassium is, therefore, not only restricted to described above facilitation of the electron transfer activation of N_2O in the first step (by lowering the catalyst work function), but is also beneficial for the preferred suprafacial pathway of O—O bond formation (deduced from isotopic experiments). In all cases these effects were most pronounced for the carbonate precursor.

4. Conclusions

The effect of potassium addition from different precursors (K_2CO_3, KNO_3, CH_3COOK, KOH) on the catalytic activity of cobalt spinel in N_2O decomposition was studied and interpreted in terms of two factors: facilitation of N_2O activation via dissociative electron transfer related to work function decrease, and promotion of suprafacial oxygen recombination. Among all the precursors, the highest promotional effect was observed for K_2CO_3, which was assigned to the highest surface dispersion and stability of potassium promoter, tuning the active sites constituted by octahedral cobalt for enhanced deN_2O catalytic activity. The results presented in this paper can be thus used as a guideline for an optimization based on a surface modifications by alkali of new catalysts for the decomposition of N_2O.

Acknowledgements

This work was sponsored by Polish National Science Centre decision number DEC-2011/03/B/ST5/01564.

The research was partially carried out with the equipment purchased thanks to the financial support of the European Regional Development Fund in the framework of the Polish Innovation Economy Operational Program (contract no. POIG.02.01.00-12-023/08).

Appendix A. Supplementary data

Supplementary data associated with this article can be found, in the online version, at http://dx.doi.org/10.1016/j.apcatb.2013.01.068.

References

[1] J. Pérez-Ramírez, F. Kapteijn, K. Schöffel, J.A. Moulijn, Applied Catalysis B 44 (2003) 117–151.
[2] S. Alini, F. Basile, S. Blasioli, C. Rinaldi, A. Vaccari, Applied Catalysis B 70 (2007) 323–392.
[3] F. Kapteijn, J. Rodriguez-Mirasol, J.A. Moulijn, Applied Catalysis B 9 (1996) 25–64.
[4] K. Omata, T. Takada, S. Kasahara, M. Yamada, Applied Catalysis A 146 (1996) 255–267.
[5] L. Yan, T. Ren, X. Wang, D. Ji, J. Suo, Applied Catalysis B 45 (2003) 85–90.
[6] L. Yan, T. Ren, X. Wang, Q. Gao, D. Ji, J. Suo, Catalysis Communications 4 (2003) 505–509.
[7] C. Ohnishi, K. Asano, S. Iwamoto, K. Chikama, M. Inoue, Catalysis Today 120 (2007) 145–150.
[8] K. Asano, C. Ohnishi, S. Iwamoto, Y. Shioya, M. Inoue, Applied Catalysis B 78 (2008) 242–249.
[9] P. Stelmachowski, G. Maniak, A. Kotarba, Z. Sojka, Catalysis Communications 10 (2009) 1062–1065.
[10] F. Zasada, P. Stelmachowski, G. Maniak, J.-F. Paul, A. Kotarba, Z. Sojka, Catalysis Letters 127 (2009) 126–131.
[11] N. Pasha, N. Lingaiah, P. Siva Sankar Reddy, P.S. S. Prasad, Catalysis Letters 118 (2007) 64–68.
[12] G. Maniak, P. Stelmachowski, F. Zasada, W. Piskorz, A. Kotarba, Z. Sojka, Catalysis Today 176 (2011) 369–372.
[13] L. Obalová, G. Maniak, K. Karásková, F. Kovanda, A. Kotarba, Catalysis Communications 12 (2011) 1055–1058.
[14] W. Hai-Peng, L. Wen-Jing, G. Li, P. Yan-Fei, X. Xiu-Feng, Journal of Fuel Chemistry and Technology 39 (2011) 550–555.
[15] A. Kotarba, I. Kruk, Z. Sojka, Journal of Catalysis 211 (2001) 265–272.
[16] O. Levenspiel, Chemical Reaction Engineering, third ed., John Wiley & Sons, New York, 1999.
[17] EUROKIN_fixed-bed_html, EUROKIN spreadsheet on requirements for measurement of intrinsic kinetics in the gas-solid fixed-bed reactor, 2012, www.eurokin.org
[18] L. Obalová, K. Jirátová, K. Karásková, F. Kovanda, Chinese Journal of Catalysis 32 (2011) 816–820.
[19] W. Piskorz, F. Zasada, P. Stelmachowski, O. Diwald, A. Kotarba, Z. Sojka, Journal of Physical Chemistry C 115 (2011) 22451–22460.
[20] L. Obalová, V. Fíla, Applied Catalysis B 70 (2007) 353–359.
[21] L. Lutterotti, D. Chateigner, S. Ferrari, J. Ricote, Thin Solid Films 450 (2004) 34–41.
[22] K. Asano, C. Ohnishi, S. Iwamoto, Y. Shioya, M. Inoue, Applied Catalysis B 78 (2007) 242–249.
[23] M. Sun, L. Wang, B. Feng, Z. Zhang, G. Lu, Y. Guo, Catalysis Today 175 (2011) 100–105.
[24] V.G. Hadjiev, M.N. Iliev, I.V. Vergilov, Journal of Physics C 21 (1988) L199–L201.
[25] J. Kreisel, G. Lucazeau, H. Vincent, Journal of Solid State Chemistry 137 (1998) 127–137.
[26] Z.V. Marinkovic Stanojevic, N. Romcevic, B. Stojanovic Journal of the European Ceramic Society 27 (2007) 903–907.
[27] G. Maniak, P. Stelmachowski, J.J. Stanek, A. Kotarba, Z. Sojka, Catalysis Communications 15 (2011) 127–131.
[28] J. Portier, H.S. Hilal, I. Saadeddin, S.J. Hwang, M.A. Subramanian, G. Campet, Progress in Solid State Chemistry 32 (2004) 207–217.
[29] P. Pietrzyk, F. Zasada, W. Piskorz, A. Kotarba, Z. Sojka, Catalysis Today 119 (2007) 219–227.
[30] W. Piskorz, F. Zasada, P. Stelmachowski, A. Kotarba, Z. Sojka, Catalysis Today 137 (2008) 418–422.